Sci. Dril., 32, 27–42, 2023
https://doi.org/10.5194/sd-32-27-2023

Scientific Drilling
Open Access

Drilling into a deep buried valley (ICDP DOVE): a 252 m long sediment succession from a glacial overdeepening in northwestern Switzerland

Sebastian Schaller[1,2], **Marius W. Buechi**[1,2], **Bennet Schuster**[3,1,2], **and Flavio S. Anselmetti**[1,2]

[1]Institute of Geological Sciences, Universität Bern, Baltzerstr. 1+3, 3012 Bern, Switzerland
[2]Oeschger Centre for Climate Change Research, Universität Bern,
Hochschulstrasse 4, 3012 Bern, Switzerland
[3]Institute of Earth and Environmental Sciences, University of Freiburg,
Tennenbacher Str. 4, 79106 Freiburg, Germany

Correspondence: Sebastian Schaller (sebastian.schaller@geo.unibe.ch)

Received: 17 March 2023 – Revised: 12 July 2023 – Accepted: 9 August 2023 – Published: 26 October 2023

Abstract. The modern Alpine landscape and its foreland were strongly impacted by the numerous glacier advance and retreat cycles during the Middle-to-Late Pleistocene. Due to the overall erosive character of each glaciation cycle, however, direct traces of older glaciations tend to be poorly preserved within the formerly glaciated domains of the pan-Alpine area. Nevertheless, sediments of older glaciations may occur hidden under the modern surface in buried glacially overdeepened troughs that reach below the normal level of fluvial erosion (fluvial base level). These sedimentary archives, partly dating back to the Middle Pleistocene period, are of great scientific value for reconstructing the timing and extent of extensive Alpine glaciation, paleoclimate, and paleoenvironmental changes in the past and help to better understand ongoing and future changes in the pan-Alpine area. Therefore, the International Continental Scientific Drilling Program (ICDP) project DOVE (Drilling Overdeepened Alpine Valleys) targets several of these glacial overdeepened sedimentary basins to recover their sedimentary infills. In the frame of the DOVE project, a 252 m long drill core of unconsolidated Quaternary sediments was recovered in northern Switzerland from an over 300 m deep glacially overdeepened structure ("Basadingen Trough") formed by the former Rhine Glacier lobe system. The recovered sedimentary succession was divided into three stratigraphic units on the basis of lithological and petrophysical characteristics. The lowest unit, deposited below the fluvial base level, consists of an over 200 m thick succession of glacial to (glacio)lacustrine sediments and contains remains of possibly two glaciation cycles. Overlying this lowermost succession, an ∼37 m thick fluvial-to-glaciofluvial gravel deposit occurs, which correlates to a locally outcropping Middle Pleistocene formation ("Buechberg Gravel Complex"). The sediment succession is capped by an ∼11 m thick diamictic succession interpreted as the subglacial till from the later extensive glaciation, including the regional glaciation during the Last Glacial Maximum. The recovered sediment succession thus supports the proposed multi-phase origin of trough formation and its infill.

1 Introduction

The global marine isotope records reveal the changes in the global temperature and ice volumes during the Quaternary. This geological period is dominated by glacial–interglacial cycles, each including stadial–interstadial higher-frequency fluctuations (Lisiecki and Raymo, 2005). Further, the marine isotope records show a global shift in the periodicity from ca. 41 to 100 ka and an increase in the amplitude of the temperature and ice volume during the Middle Pleistocene climatic transition (MPT) between 1250 and 700 ka (Ruddiman et al., 1986; Clark et al., 2006). During each glacial–interglacial cycle, ice sheets grew in the polar areas as well as in mountainous areas (including the Alps), and glaciers advanced into

the lowlands from where they retreated again with the onset of the next interglacial. While the last glaciation left prominent traces in the Alpine landscape (e.g., erratic blocks and side and end moraines), traces of previous glaciations often became obscured and eroded as advancing glaciers modified the overridden landscape drastically.

During extensive glaciation of the Alpine foreland, numerous glacially overdeepened troughs were eroded by subglacial processes below the fluvial base level, i.e., below the lowest fluvial channels terminating downstream with adverse slopes (e.g., Cook and Swift, 2012; Alley et al., 2019). Upon deglaciation, the troughs were refilled with sediments and, in most cases, eventually completely buried. Like this, the valley fills remained at least partially protected from subsequent glacial and fluvial erosion and therefore contain relatively complete or multi-phase archives extending through several glacial cycles (Preusser et al., 2010; Ellwanger et al., 2011; Pomper et al., 2017; Buechi et al., 2018). Therefore, these overdeepened valley fills represent some of the most valuable land-based sedimentary archives in glacial landscapes for reconstructing glacial history over multiple glaciations. They thus contribute significantly to reconstructing the glaciation history preceding the last glacial cycle in areas such as the Alps and its foreland, as shown in several case studies (Dehnert et al., 2012; Fiebig et al., 2014; Buechi et al., 2018; Schwenk et al., 2022). These studies profited from new developments in dating methods, especially luminescence dating and cosmogenic nuclide burial dating, which allow researchers to establish an absolute chronology of those archives, which is a prerequisite for understanding and reconstructing the local-to-regional glaciation history into a broader context. On a regional scale, the onset of increased glacial erosion (Haeuselmann et al., 2007; Valla et al., 2011) and the beginning formation of overdeepened structures during the MPT have been proposed for the Alpine region at that time (e.g., Schlüchter, 2004; Ellwanger et al., 2011). The initial concept with four proposed Alpine glaciations (Penck and Brückner, 1909) has been replaced by a scenario with ca. 15 proposed glaciations (Preusser et al., 2011). Furthermore, it has been documented that regional the glacial dynamics and extents also vary strongly inside the pan-Alpine area. For example, it is postulated that at around ca. 65 ka, the glaciers in the western Alps reached their last maximum of extension (e.g., Gribenski et al., 2021), while it is postulated that glaciers barely reached into the inner Alpine valleys in the Eastern Alps (Ivy-Ochs et al., 2008). Such asymmetry and asynchronicity can be related to many local, regional, and global factors such as topography, climate change (including temperature and precipitation), and ice dynamics (e.g., Reber and Schlunegger, 2016; Spötl et al., 2021).

All these studies also underline the potential and justify the significant logistical and financial effort to drill, document, and analyze these overdeepened troughs and their sediment fill. Besides their unique scientific value as sedimentary archives, understanding overdeepened structures is also crucial for applied aspects such as the longtime safety of nuclear waste disposal sites, groundwater reservoirs, natural hazards, and large-scale underground transportation infrastructure.

Project DOVE

In the frame of the International Continental Scientific Drilling Program (ICDP) project Drilling Overdeepened Alpine Valleys (DOVE), the sedimentary infill of several overdeepened troughs are targeted with the overarching goal of quantifying the proposed asymmetry in the extent and timing of the Alpine glaciations in the pan-Alpine area and their implications for the paleoclimate, paleolandscape, and paleoenvironmental evolution back to the Middle Pleistocene. A detailed overview of the DOVE project is provided in Anselmetti et al. (2022). The project seeks to achieve these goals by combining the following: (i) a series of new drill cores, (ii) analyzing existing drill cores, and (iii) geophysical surveys across overdeepened troughs. The project is grouped into two phases: Phase I covers the northern and northeastern parts of the Alps (Switzerland, Germany, and Austria) and comprises three drill cores from the former Rhine Glacier area (ICDP Site 5068_1, TANN, IGSN (International Generic Sample Number): ICDP5068EH70001; ICDP Site 5068_2, BASA, IGSN: ICDP5068EH40001; and ICDP Site 5068_6, GAIS, IGSN: ICDP5068EHG0001; Fig. 1a), one from the former Isar-Loisach Glacier area (ICDP Site 5068_3, SCHA, IGSN: ICDP5068EHC0001), one from the former Salzach Glacier area (ICDP Site 5068_4, FREI, IGSN: ICDP5068EHD0001), and one from the former Traun Glacier area (ICDP Site 5068_5, BADA, IGSN: ICDP5068EHE0001) (Anselmetti et al., 2022). It is planned to cover the southern and western parts of the Alps (Slovenia, Italy, and France) in Phase II (Anselmetti et al., 2022). The comparison and integration of data in Phase I will occur in several steps: (i) the data of the individual drill cores will be individually analyzed and integrated into the local context; (ii) the sites will be integrated into their extended regional system, e.g., the individual glacier lobes; and (iii) an overall synthesis of Phase I in the northern Alps will be accomplished. Eventually, the same steps are planned for Phase II for the southern and western areas. Finally, the overall DOVE synthesis and integration over the entire pan-Alpine area will be achieved. This study represents the first step on this path and presents the results of the ICDP site 5068_2 (BASA), where the first ICDP drill core was recovered on Swiss territory (Fig. 1a and b).

2 Study area

The study area is located in the southwestern part of the former Rhine Glacier lobe and inside the proposed Most Extensive Glaciation (MEG) during the Middle Pleistocene and the Last Glacial Maximum (LGM, Fig. 1a). Previous studies have documented a dendritic pattern of overdeepenings

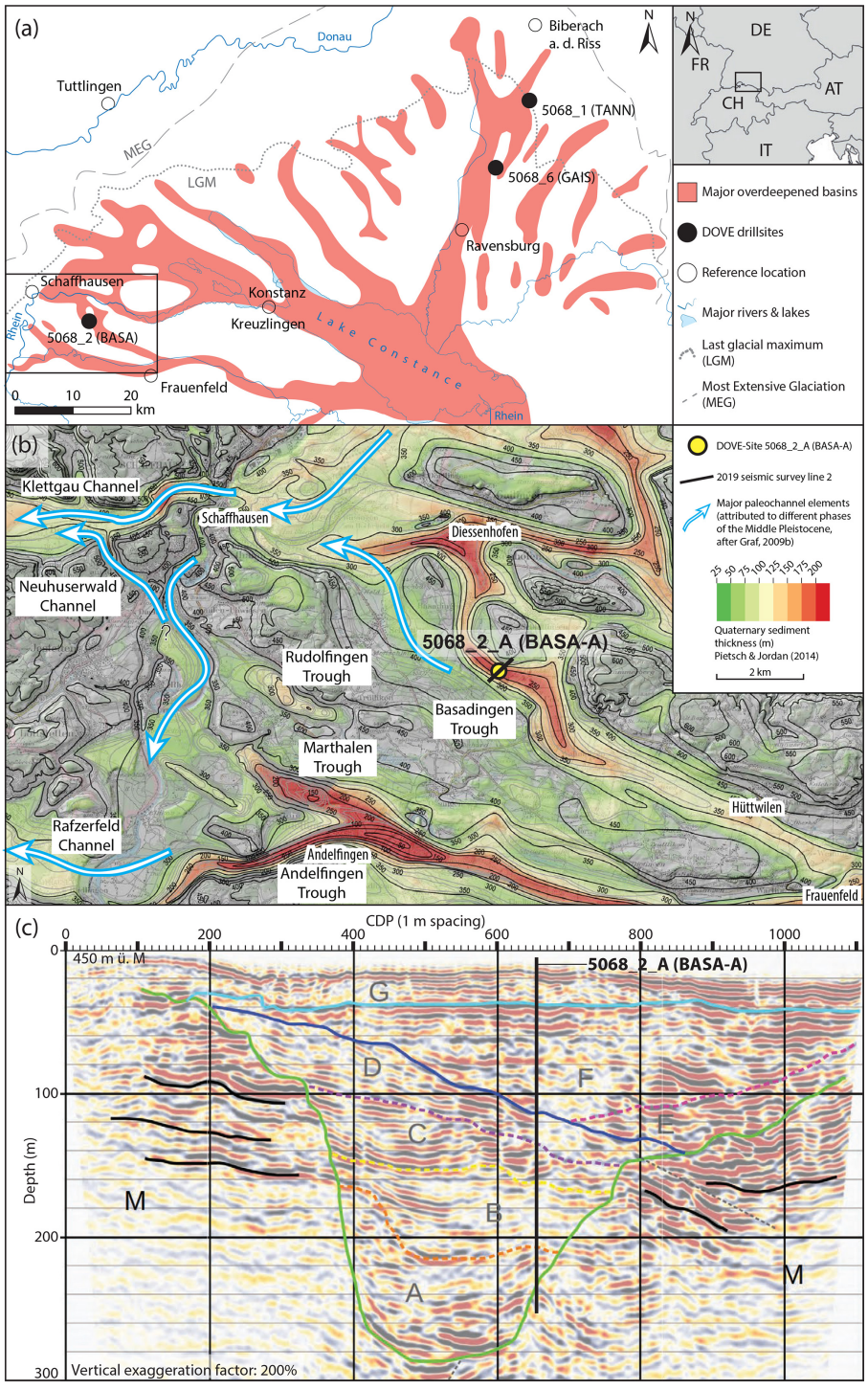

Figure 1. **(a)** Overview of the overdeepened systems within the former Rhine paleoglacier lobe (modified from Ellwanger et al., 2011). Extents of the Rhine Glacier during the Most Extensive Glaciation (MEG) and of the Last Glacial Maximum (LGM) and two DOVE Phase 1 sites: 5068_1 (TANN), 5068_2 (BASA), and 5068_6 (GAIS) are indicated. **(b)** Regional overview of the overdeepened system of the southwestern branch of the Rhine Glacier, including the thickness of the Quaternary sediments (Pietsch and Jordan, 2014), the postulated local Middle Pleistocene paleochannels (Graf, 2009b), the indicated DOVE site 5068_2 (BASA), and trace of the seismic line. **(c)** Pre-drilling interpretation of the seismic line across the Basadingen Trough (Brandt, 2020): M represents the molasse bedrock; the green line represents the outline of trough; A–G represent the stratified unconsolidated Quaternary filling with indicated potential erosional (solid lines) and internal boundaries (dashed lines); solid black lines in M represent prominent and potential continuous reflections; dashed black lines represent assumed faults; the black vertical line represents drill hole 5068_2-A (BASA-A) with predicted bedrock at ~240 m depth. Note that the final drilling depth of 252 m did not penetrate bedrock but ended in coarse (basal) sediments.

within the footprint of the Rhine Glacier (Fig. 1a). Geometrically, these overdeepened basins appear to have a common root in the Alpine Rhine valley and the partially filled basin of Lake Constance (e.g., Keller and Krayss, 1993; Cohen et al., 2018; Ellwanger et al., 2011; Fabbri et al., 2021; Schaller et al., 2022). From this root, several overdeepened basins branch into side systems and even further distal overdeepenings (Fig. 1a). While the origin of this pattern is not fully understood, regional studies indicate that the formation of these overdeepenings did not all occur at the same time but during different glaciations (e.g., Graf, 2009a, b; Ellwanger et al., 2011; Müller, 2013).

In the surroundings of the drill site, with a terrain elevation at the drill site of ∼ 445 m above sea level (m a.s.l.), several parallel to partly cross-cutting bedrock overdeepenings have been detected in bedrock surface maps compiled from variably abundant drillings and geophysical data (Fig. 1b; e.g., Müller, 2013; Pietsch and Jordan, 2014). The bedrock overdeepenings, including the Basadingen Trough, reach over 300 m below the modern topography and are mainly incised into the Neogene siltstones and sandstones of the Molasse basin (mainly Upper Marine Molasse, OMM, and Lower Freshwater Molasse, USM; Hofmann and Hantke, 1964; Hofmann, 1967). The bedrock maps also reveal characteristic adverse slopes at the termini of the individual overdeepenings. At the surface, the considerable bedrock relief due to overdeepening glacial erosion is buried by younger glacial or glaciofluvial sediments (Graf, 2009b; Müller, 2013).

The transition from the overdeepened to non-overdeepened (fluvial) domain is an important physical process boundary for the interpretation of the erosional and depositional processes. The lowest fluvial outlet of the study area is the Klettgau fluvial paleochannel and lies at ∼ 340 m a.s.l. just west of Schaffhausen. Considering this minimal fluvial base level, the erosional and depositional processes below ∼ 100 m core depth have occurred in an overdeepened position and, thus, most likely in a subglacial-to-lacustrine setting. Higher values for the fluvial base level at the drill site – but with larger uncertainties – can be estimated from the highest elevations reached by the adverse slopes. Based on the base maps of the lowest fluvial gravels ("Buechberg Gravel Complex", Middle Pleistocene; Müller, 2013), Graf (2009b) and Müller (2013) convincingly show that the lowest Pleistocene base (LPB) level gently rises to the east and reaches ∼ 370 m a.s.l. at the lowest known basal contact of the gravel formation. The base map reveals a strong topography of this basal boundary surface, which lies between 390 and 400 m a.s.l. around the drill site.

As part of the drill site selection process, two closely spaced seismic cross-sections over the Basadingen Trough were acquired using an acoustic signal source with a frequency between 20 and 240 Hz, a shot-point spacing of 4 m, and a receiver spacing of 2 m (Brandt, 2020, Fig. 1c). The time-to-depth conversion of the two lines was based on the stacking velocity model, assuming velocities of $\sim 2500\,\mathrm{m\,s^{-1}}$ for bedrock and between ∼ 1400 and $\sim 2100\,\mathrm{m\,s^{-1}}$ for the sedimentary infill. The use of the rather simplified velocity model may have caused some uncertainties in the time–depth conversion of the seismic data. Both lines indicate a nearly 300 m deep bedrock incision and an infill which was interpreted to be a complex stratified geometry with a major cross-cutting unconformity separating a deep and narrow structure from a broad and shallow depression. This pattern suggests a multi-phase infill history during at least two glaciation cycles, as was earlier proposed by Müller (2013) based on existing flush drillings.

3 Methods

3.1 Drilling and downhole operations

Drilling operations were conducted by a private contractor (Fretus AG, Bad Zurzach, Switzerland) between 25 May and 10 November 2021 (Fig. 2a–d). A final depth of 252 m was reached using a combined approach of percussion drilling (Düsterloh hammer) to a depth of 57 m and, below, a triple-tube core-barrel system (CSK-146 wireline diamond-coring system). Bedrock, initially predicted for ∼ 240 m (Fig. 1c), could not be reached due to geotechnically challenging sediments, loss of drilling fluid in the hole, and related technical difficulties at the final depth of 252 m. The > 12 m underestimation of Quaternary sediment thickness is likely related to uncertainties in (i) the seismic velocities and/or (ii) the interpretation of the deeper reflections. A total of 278 core sections with a core diameter of 104 mm and lengths between 0.1 and 1 m were recovered in opaque PVC liners. The liners had a standard length of 1 m and were only cut if the length of the nominal drilled section was < 1 m. The liners were not cut in the case of core loss, and this space was not compensated with filler material. Consequently, the quality of those sections may have suffered due to some remobilizations, especially in cases of low internal cohesion. However, since the main reason for the core loss was mobilization and/or flushing during the drilling itself, those sections were of poor quality anyway. A total recovery of ∼ 94 % was reached, from which ∼ 11 % was disturbed to the degree that it lost its internal structure. Water inflow was registered at depths of 3–4 and 10–11 m. The local groundwater table was reached at a depth of ∼ 29.5 m, which remained stable during the entire drilling operation. Significant drilling-fluid losses occurred in gravel-dominated sections between 93–108 and 141–143 m and below 250 m. They represent the major technical and lithological challenges encountered during the drilling operation. For stabilizing and reducing the drilling resistance inside the drill hole, the drill hole was telescoped several times by using different casing diameters and a flushing agent consisting of water mixed with additions of biodegradable polymers and bentonite. After the completion of the drilling activities, a broad downhole wireline logging

campaign was executed by the Leibniz Institute for Applied Geophysics (LIAG). After completion of the wireline logging, the drill hole was refilled with intervals of gravel, bentonite, and concrete according to governmental regulations. A detailed technical overview of the drilling and logging operations; core quality; the technical parameters, such as borehole geometry, used casings, and the applied refilling scheme is provided in the DOVE operational report (DOVE-Phase 1 Scientific Team et al., 2023a).

3.2 Core handling, description, and analysis

3.2.1 On-site core-related workflow

After recovery, the liners were sealed and labeled with section ID and driller depth. Each core section was weighed for a preliminary approximation of recovery. In parallel to the drilling campaign, *p*-wave velocity (will not be further considered due to poor quality), wet bulk density, magnetic susceptibility, and natural gamma radiation of each core section were measured in the field laboratory (Fig. 3) with a Geotek multi-sensor core logger (MSCL) (Geotek Limited, Daventry, Northants, UK) at a resolution of 5 mm. The core sections were stored in labeled standard-sized wooden boxes for better handling. Later, they were brought in batches to the Institute of Geological Sciences, University of Bern, to be stored in the cooling room until the initial core description (ICD). In parallel to recovering, the fine-grained and sandy sediments were strategically sampled for noble-gas pore-water analyses (16 samples) and microbiological investigations of the deep biosphere (60 samples).

3.2.2 Off-site core-related workflow

During the ICD, each core section was cut, opened, and split lengthwise into an archive half for non-destructive analyses and a working half for invasive sampling. Complete processing of the working half was performed under red-light conditions to prevent light contamination, potentially hampering the use of optically stimulated luminescence (OSL) dating. The following work was conducted on each archive half. A high-resolution line scan was obtained, and each section was sedimentologically described and documented in a log sheet. The focus of these descriptions was on the following: (i) the dominant grain size, (ii) type and thickness of bedding, (iii) color, (iv) contacts between different beds, (v) secondary sedimentary structure, (vi) quality of the core section, and (vii) an overview of clast lithology and morphology. Furthermore, where applicable, undrained shear strength (c'_u) and undrained uniaxial compressive strength (q'_u) were measured at 25, 50, and 75 cm section depth with a pocket vane shear tester and a pocket penetrometer. A final total depth was defined based on the observations of core quality from the ICD and the driller's top depth of each section. Depth is addressed as meters total depth (mtd) when discussing the entire sediment succession or as centimeter section depth (cmsd) when aiming for individual core sections. Based on the combined findings from the ICD, 14 sedimentary lithotypes were defined and described (Table 1). The whole sediment succession was assigned to the best-fit lithotype. Eventually, the stratigraphic succession was subdivided into three main stratigraphic units (A–C).

In addition, X-ray computed tomography (CT) images of 49 selected core sections were taken with a medical X-ray CT scanner at the Institute of Forensic Medicine, University of Bern. Systematically, 231 samples for grain-size distribution, geochemical analyses (e.g., total inorganic carbon, TIC, and total organic carbon, TOC), and potential additional investigations were taken from each working half at 50 cmsd whenever possible (sample spacing ~ 1 m). These samples were freeze-dried, and the mean water content at each position was derived from the corresponding weight differences between the three wet and dry subsamples. Furthermore, smear slides have been taken from interesting silt- and clay-rich sections.

Further, based on the line scans, samples were taken for a first screening of pollen content (31 samples), luminescence dating (22 samples), cosmogenic nuclide burial dating (2 samples), and geotechnical analyses (23 samples). After completing the ICD and the sampling campaign, the core halves were sealed in lightproof black foil, stored in standard-sized wooden boxes, labeled according to the ICDP guidelines, and brought to a commercial cooled storage facility, which serves as a temporary repository during the active DOVE Phase I (Anselmetti et al., 2022). For further information on the curated samples, analysis, and data, see the operational dataset (DOVE-Phase 1 Scientific Team et al., 2023b) and explanatory remarks (DOVE-Phase 1 Scientific Team et al., 2023c).

3.2.3 Carbon analysis (organic matter and carbonate content)

Total carbon (TC), nitrogen, sulfur, and total inorganic carbon (TIC) were analyzed from the fine fraction (< 63 µm) using a Thermo Scientific FLASH 2000 elemental analyzer (Thermo Fischer, Waltham, MA, USA). Total organic carbon (TOC) was derived as the differences between TC and TIC. Weight percent of carbonates ($CaCO_3$) and organic matter were calculated using a stoichiometrically simplified approach from TIC and TOC through multiplication with 8.3 and 1.8, respectively (Meyers and Teranes, 2001). This approach does not consider potential down-core changes in carbonate phases (i.e., dolomite / carbonate ratio). Nevertheless, it allows for a quantitative approximation of the total lithological constituents.

3.2.4 MSCL data processing

MSCL data were processed in five steps: (i) data of empty sections of liners, representing core loss, were removed; (ii) a baseline correction was applied to the corresponding mag-

Figure 2. **(a)** Drill rig used from 0 to 228 mtd (meters total depth); **(b)** drill rig used from 228 to 252 mtd; **(c)** drill bit used during percussion-hammer coring to a depth of 57 mtd; and **(d)** diamond and hard-metal drill bit used during rotary drilling below 57 mtd (photos by Sebastian Schaller).

Figure 3. Field lab near the drill site containing the MSCL scanner (photo by Sebastian Schaller).

netic susceptibility data to correct potential systematic shifts in the data (subtraction of the average of the calibration data between 0.5 and 15 cm of each measurement cycle); (iii) low-density data ($< 1.5\,\mathrm{g\,cm^{-3}}$), considered heavily disturbed sections, were excluded from the density log; (iv) *p*-wave velocity data with an amplitude of 0, representing poor data quality, were excluded from the *p*-wave data (As the overall data quality of the *p*-wave data is low, *p*-wave-velocity values are not further presented or discussed.); (v) the depth of the cleaned MSCL logs was corrected with the actual depth; and (vi) the data from the uppermost and lowermost centimeter in each section were considered likely disturbed and thus excluded.

4 Results

4.1 Core lithologies

The 252 m long sediment succession was divided into 14 sedimentological lithotypes (Fig. 4). Table 1 provides an overview of these 14 defined lithotypes, including description and interpretation of the depositional environment, along with a representative core-section line scan. Figure 5 displays a composition of detailed line scans, CT scans, and the key lithotypes of 10 selected core sections.

4.2 Lithostratigraphic units

Based on the succession of the 14 endmember lithotypes (Table 1), the recovered succession (Fig. 4) was grouped into three lithostratigraphic units (A, B, and C), with Unit A containing five subunits (A1–A5). These units are briefly characterized from bottom to top.

Table 1. Colors and lithocodes of the individual lithotypes with description and interpretations. The line-scan image shows a representative core section (origin of line scan is indicated in the lower-right corner of core photos); scale is in centimeters.

	Description	Interpretation	Core photo
	Diamicts		
Dmm	***Matrix-supported massive:*** Massive matrix-supported with isolated fine to coarse gravel clasts in a silty to sandy matrix with isolated cobbles (0-40 % clasts, 60-100 % matrix). Crudely bedded in decimeter- to meter-scale by a slight variation in matrix composition and/or in clast size and number. Beige color, many fresh striations, poorly sorted, subangular to subrounded.	i) Subglacial till (Evans et al., 2006) or ii) terrestrial or subaqueous cohesive debris flows with glacial sediment sources (Mulder and Alexander, 2001; Eyles et al., 1983).	
Dms	***Matrix-supported stratified diamict:*** Matrix supported with fine to coarse gravel clasts in a massive sandy to partly silty matrix (0-40 % clasts, 60-100 % matrix), stratified into centimeter- to decimeter-scale beds by oriented but mostly isolated clasts. Beige to grey-beige color, few striations, poorly sorted, subangular to (sub)rounded.	Proximal hyperconcentrated density flow deposits (Mulder and Alexander, 2001).	
Dcm	***Clast-supported massive diamict:*** Massive clast-supported, fine to coarse gravel with isolated cobbles with a silty matrix with variable sand content (60-80 % clasts, 20-40 % matrix). Sometimes crudely bedded by a slight variation in matrix composition and dominant clast size. Poorly sorted, beige matrix color, striations, subangular to subrounded.	i) subglacial below or above the fluvial base level (Evans et al., 2006), or ii) glaciofluvial deposits solely above the fluvial base level (Eyles et al., 1983).	
Mcc	***Mud-clast conglomerate:*** Mixture of beige to beige-brown clay chips with a variable medium to coarse gravel content (0->50%) in a grey-beige to brownish medium sandy matrix (5-80 % clasts, 20-95 % matrix). Mud clasts show partially internal structures and rounding of various degrees (subangular to rounded).	Fine lacustrine sediments, rounding indicates transportation upon reworking, eroded by subaquatic mass movements or other subaquatic events with high erosive potential (e.g., Li et al., 2017). The individual gravel content may indicate the type of event, i.e., a high content may indicate a delta collapse as source event.	
	Gravels		
Gms	***Massive to crudely bedded sandy gravel:*** Massive medium to coarse (partly fine) gravel, with few isolated sand layers, with little to no silt and isolated cobbles (75-80 % clasts, 20-25 % matrix). Crudely bedded by variation in clast size and number and slight variation in matrix composition, moderately to well sorted, beige to beige-brownish matrix color, (sub)rounded to well rounded.	i) Fluvial to glaciofluvial deposits (over the fluvial base level; Eyles et al., 1983) or ii) subglacial to glaciolacus- trine deposits, e.g., high concentration channelized density flows in a subaqueous glacial fan system (below the fluvial base level; Eyles et al., 1983).	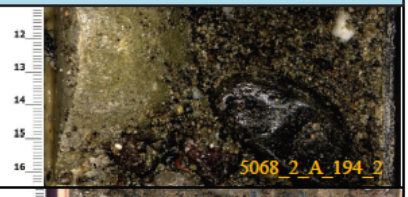
Gmf	***Massive to crudely bedded silty sandy gravel:*** Massive medium to coarse gravel, partly sandy, silty with isolated cobbles (75-80 % clasts, 20-25 % matrix). Crudely bedded by variations in clast size and number and slight variations in matrix composition, moderately to well sorted, brownish-reddish to brownish matrix color, (sub)rounded to well rounded, with some cementations and oxidations.	Fluvial to glaciofluvial deposits (Eyles et al., 1983), in the range of current groundwater fluctuations, leads to cementation and oxidations of clasts.	
	Fines		
Fm	***Massive clay/silt:*** Massive clay and silt, little sandy, only very few isolated gravel clasts (C: <1 %, M: >99 %). Partially laminated by intercalating sand laminae resulting in a centimeter- to decimeter-scaled bedding, rarely mottled by soft clasts, with some isolated drop stones, well to very well sorted, beige to grey beige, partly slightly brownish.	i) Deposited in calm states of the lake, i.e., (glacio)lacustrine background sedimentation (Leemann and Niessen, 1994). ii) the very top of a concentrated density flows event (Mulder and Alexander, 2001); or iii) very distal from the sediment source or low energy turbidity deposits (T_e, Bouma 1962).	

4.2.1 Unit A: 252.00–47.75 mtd

Unit A consists of primarily sand-dominated sediments (Fig. 5c–j) intercalated by several-meter-thick gravel-dominated beds (Fig. 4). The sand-dominated successions can be distinguished and categorized into three types: (i) stacked massive sandy beds with low clay and silt content (Table 1; *Sm* and *Sh*), partially separated by clay caps (*Fm*), and intercalated by isolated minor gravel beds (*Gms*) or gravel-rich sections (*SGm*); (ii) fine-to-medium sand beds

Table 1. Continued.

	Description	Interpretation	Core photo
	Sands		
Sm	***Massive sand:*** Massive fine to medium sand, occasionally coarse sandy, with little to no silt and only isolated gravel clasts (<5 % clasts, >95 % matrix). Crudely bedded in decimeter- to meter-scale by a slight variation in silt content and dominant grain-size fraction, well to very well sorted, greyish-beige to brownish-beige, rarely mottled with soft clasts.	Hyperconcentrated density flow deposits (Mulder and Alexander, 2001).	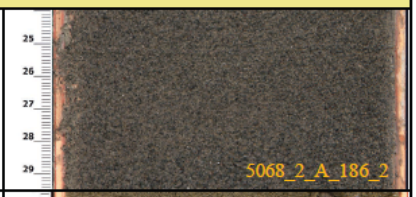 5068_2_A_186_2
SGm	***Massive sand and gravel mix:*** Massive mix of fine to medium sand and gravel, with little to no silt (5-60 % clasts, 40-95 % matrix). Partly centimeter- to decimeter-scale bedded by oriented clasts, moderately to well sorted, subrounded to well rounded, greyish-beige to brownish-beige.	Base of concentrated density-flow deposits, very proximal to sources, or high-energy events (Mulder and Alexander, 2001).	 5068_2_A_137_1
Sh	***Bedded sand:*** Bedded fine to medium sand, with variable silt content and few isolated gravel clasts (<5 % clasts, >95 % matrix). Bedded in centimeter- to decimeter-scale by a variation in silt content and dominant grain-size fraction, fining up to a massive appearance, well to very well sorted, greyish-beige to brownish-beige.	i) (Massive) hyperconcentrated density flow deposits (Mulder and Alexander 2001), more distal to the source or with less energy, or ii) (stratified) turbidity deposits (T_a; Bouma, 1962; Mulder and Alexander, 2001).	 5068_2_A_079_1
Sl	***Laminated sand:*** Laminated fine to medium sand with variable silt content, with few isolated clay laminae and isolated gravel clasts (<1 % clasts, >99 % matrix), laminated in millimeter- to centimeter-scale by variations in silt content and dominant grain-size fraction. Individual laminae are fining-up to massive, partially mica-rich, well to very well sorted, greyish-beige to brownish-beige, with partially reddish colors.	Distal or low-energy turbidite deposit (T_b, T_d; Bouma, 1962).	 5068_2_A_159_1
Sc	***Cross-bedded sand:*** Cross-bedded fine to medium sand, partially silty, with isolated clay laminae and very few isolated gravel clasts (<1 % clasts, >99 % matrix). Cross-bedded in centimeter- to decimeter-scale with internal millimeter-scaled laminae, individual laminae are fining up, partly mica-rich, well to very well sorted, greyish-beige to brownish-beige, occasionally of reddish color.	Distal or low energy turbidity deposit (T_c; Bouma, 1962).	 5068_2_A_067_1
Sil	***Irregularly bedded sand, silt, and clay:*** Silt and clay to coarse sand, with individual gravel clasts (0-10 % clasts, 90-100 % matrix). Irregular in centimeter- to sub-decimeter-scale bedded to laminated, individual lamina/beds are mostly well-sorted and are massive to partly fining-up, partially deformed, with internal erosive contacts, with high contrast, greyish beige to brownish beige.	Stacked successions of different types of density-flow deposits, likely formed under highly variable energy conditions, possibly in cross-cutting subaquatic channel systems.	 5068_2_A_089_1
Sd	***Deformed mix of sand, silt, and clay:*** Strongly folded and bent mix of originally laminated to bedded sand, clay, and silt with isolated gravel clasts (<1 % clasts, >99 % matrix). Traces of slumps and dehydration structures, ductile deformed, beige to brownish beige.	i) Deformed syn- or postdepositionally by i) rapid loading and dewatering or, ii) mass movements, or iii) glaciotectonics (Evans, 2018).	 5068_2_A_163_2

with a higher clay and silt content, thin-bedded (*Sh*) to laminated (*Sl*) and partially cross-bedded (*Sc*), and with isolated clay laminae (*Fm*); and (iii) massive sand (*Sm, Sh, Sl,* and *Sil*) interbedded to intercalated with mostly centimeter-to-decimeter-scaled partly stratified beds of sand and gravel mix (*SGm*), massive gravel beds (*Gms*), and stratified (*Dms*) or massive diamictic (*Dmm*) beds. The sandy successions, in parts, show traces of ductile deformations (Table 1; *Sd*, e.g., boudinage, flame structures, folding, and dewatering structures) and some brittle deformation (e.g., small-scale faults). The bases of the rather massive sandy or gravel-rich beds partially show erosive contacts, which may contain rip-up clasts (*Mcc*).

The gravel-dominated beds within Unit A can be further divided into two types: (i) more diamictic beds (Table 1; *Dcm*) with a silt-rich matrix, steeply inclined beds,

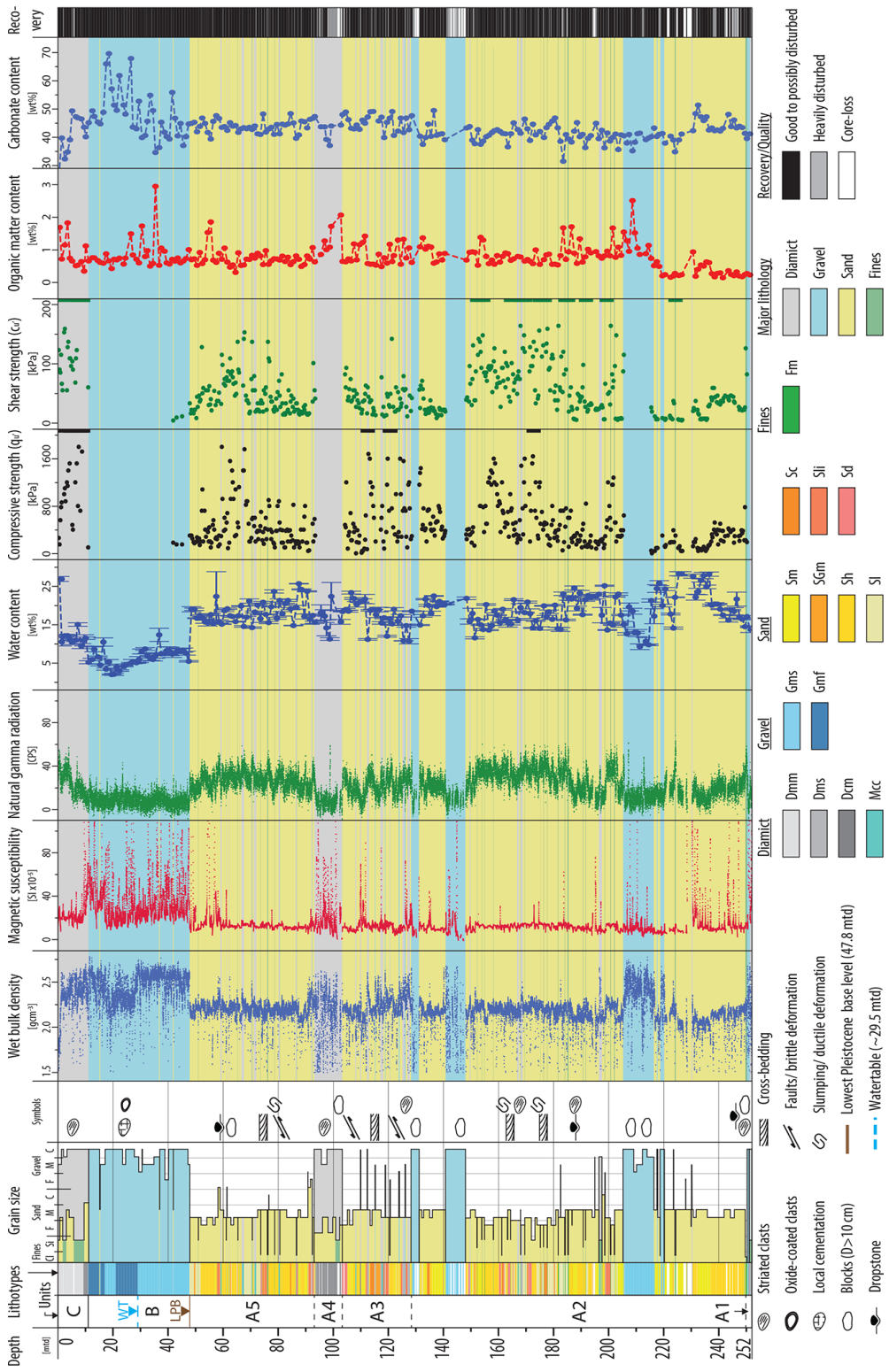

Figure 4. Lithological and petrophysical data versus depth. Columns from left to right: depth-scale [mtd], stratigraphic units (labeled with A1–A5, B, and C; WT = water table; LPB = lowest Pleistocene base level), lithotypes, dominant grain size with indicated main lithotypes, symbols of prominent observations, wet bulk density ($g\,cm^{-3}$), magnetic susceptibility ($SI \times 10^{-5}$), natural gamma radiation (CPS, counts per second), water content with indicated standard deviation (wt %), undrained uniaxial compressive strength (q_u') (kPa), undrained shear strength (c_u') (kPa), organic matter content (wt %), carbonate content (wt %), and the recovery. Main lithotypes are indicated as semi-transparent color codes over the plot's entire width.

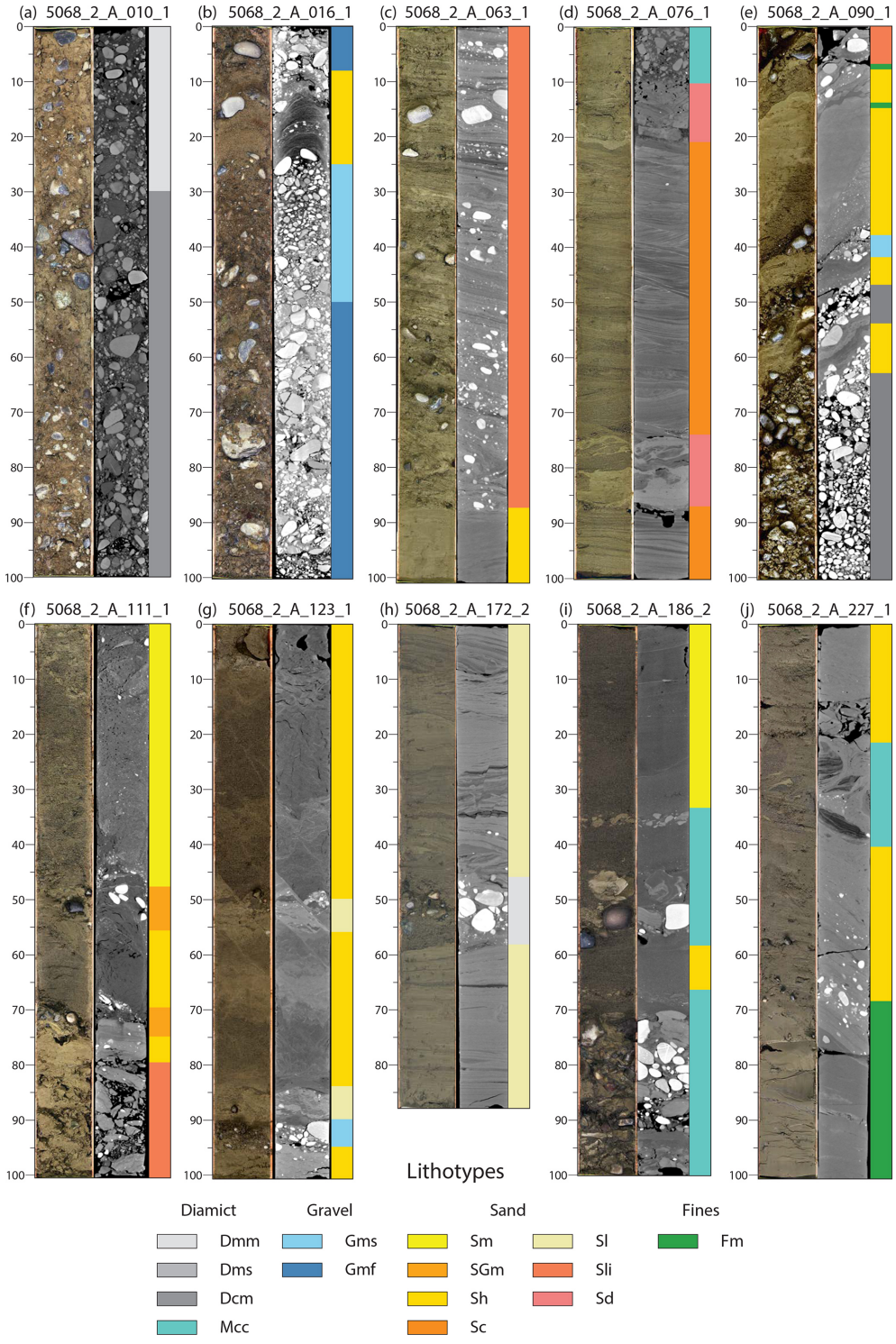

Figure 5. CT and line scans of selected representative core sections with corresponding lithotypes. Each core section is labeled at the top; the scale is in centimeter section depth (cmsd) and shows the following from left to right: line scan, CT scan, and lithotypes. The color code for the lithotypes is given at the bottom. Shown core sections from left to right are the following: **(a)** 5068_2_A_010_1 (9–10 mtd), **(b)** 5068_2_A_016_1 (15–16 mtd), **(c)** 5068_2_A_063_1 (58–59 mtd), **(d)** 5068_2_A_076_1 (74–75 mtd), **(e)** 5068_2_A_090_1 (93–94 mtd), **(f)** 5068_2_A_111_1 (111–112 mtd), **(g)** 5068_2_A_123_1 (122–123 mtd), **(h)** 5068_2_A_172_2 (182–182.88 mtd), **(i)** 5068_2_A_186_2 (196–197 mtd), and **(j)** 5068_2_A_227_1 (249–250 mtd).

and, in parts, including striated and bullet-shaped clasts and (ii) gravel beds (*Gms*) with better clast rounding, low silt and clay content, and a primarily sandy matrix. The base of Unit A (> 249.7 mtd) is built by a succession of diamictic beds with a massive dropstone-rich ~ 0.5 m thick clay bed on top (*Fm*; Fig. 5j). Several larger Molasse bedrock fragments and clasts with glacial striations occur in this diamictic succession. Additionally, some coarse-grained sections have a high permeability as large volumes of fluids were lost during drilling.

Over the entire Unit A, the sandy sections generally show lower density and magnetic susceptibility values and higher natural gamma values than gravelly ones (Fig. 4). Organic matter content varies between 0.5 % and 1 % except from some isolated peaks of up to 2 % in the sandy sections and a drop to nearly 0 % below 217 mtd. The carbonate content ranges between ~ 40 % and 50 %.

4.2.2 Unit B: 47.75–11.00 mtd

Unit B consists of a succession of decimeter-to-meter-thick beds of sandy (Table 1; *Gms*) to partly silty (*Gmf*) gravel with isolated sand beds. The gravel beds are well sorted to locally moderately sorted with a clast-size range from fine to coarse gravel with some cobbles, and clasts are mostly (sub-)rounded to well-rounded. The groundwater table separates the succession of Unit B into the following: (i) below ~ 29.5 mtd, constantly water saturated and with a sand-rich and silt-and-clay-poor matrix, and (ii) above ~ 29.5 mtd, affected by the fluctuation of the groundwater table, with local cementations and oxide-covered clasts and a partly silt- and clay-enriched matrix (Fig. 5b). The section generally has a high density with stepwise changes above the groundwater table, high but noisy magnetic susceptibility values, and low natural gamma values (Fig. 4). Furthermore, Unit B has a low organic matter content of ~ 1 % and a highly variable carbonate content between 35 % and 65 %.

4.2.3 Unit C: 11.00–0.00 mtd

The uppermost unit consists mainly of a massive to crudely bedded, poorly sorted, silty to partly sandy matrix-supported diamict (Table 1; *Dmm*; Fig. 5a) with a clast-size range from fine gravel up to cobbles and a frequent appearance of striated and/or bullet-shaped/flat-iron-shaped clasts. A general fining-up trend occurs in the clast size together with a decrease in clast content from ~ 80 % to > 5 %, supported by the up-core decreasing trend of the density values and the negatively corresponding natural gamma log (Fig. 4). The uppermost ~ 1 m shows an increasing level of organic matter, decalcification, signs of bioturbation, and a humus layer on its very top.

5 Interpretation and discussion

5.1 Interpretation of depositional environment

5.1.1 Unit A (252.00–47.75 mtd): overdeepened basin fill

The sediments of Unit A were deposited in an overdeepened setting in a clastic-dominated glacial, glaciolacustrine, or lacustrine environment. The thick, stacked succession of current and mass-movement-dominated lithotypes suggests that the overdeepening was the depocenter and dominated by fast accumulation forming deltaic or basin-floor fan systems (Table 1). In such a setting, the observed lithotype association with thick sandy successions (mainly *Sm* and *Sh*), interbedded gravels (*Gms*), and gravelly diamicts (*Dms, Dcm,* and *Mcc*) may be interpreted as an externally forced system driven by allogenic or autogenic processes. In the case of an autogenic endmember, the activity and proximity of the sediment influx from the glacier or rivers exert the dominant controls defining the primary sediment and energy source (e.g., Lønne, 1995; Fitzsimons and Howarth, 2018). Thus the changes in the grain-size distribution and the thickness of the bedding may represent changes in the glacier's position. However, since these energy changes are not instantaneous but occur gradually over a longer time, other processes are needed to explain the frequently observed grain-size variations. Alternatively, accumulation on proximal basin-floor fan systems is associated with considerable lateral facies variability, reflecting allogenic changes of the deposition on basin-floor fans (Lønne, 1995; Fitzsimons and Howarth, 2018). This would partly suppress the sedimentary traces of the glacial proximity-related long-term depositional environmental changes, especially the potential shift from a glaciolacustrine towards a more lacustrine regime. Nevertheless, with an increasing distance of the glacier, the dominant depositional environment will evolve from a direct glacial, via a glaciolacustrine, to a lacustrine one, which may even develop into a warm lake state until the next glacial advance will reverse the evolution (e.g., Fitzsimons and Howarth, 2018; Dehnert et al., 2012; Anselmetti et al., 2022). On the basis of these processes, the succession of depositional environments of Unit A is subdivided into five subunits (from bottom to top, A1–A5):

- *Subunit A1 (> 249.7 mtd).* The basal diamictic succession (Table 1; *Dmm, Dcm*, and *Fm*) is interpreted as proximal, submarginal to possibly subglacial deposits, emplaced in close proximity to a glacier grounded in the deep trough. The interpretation is supported by the pervasive occurrence of striated clasts and the strongly inclined bedding, indicating glaciotectonic processes. The large number of local bedrock fragments in the basal succession indicates proximity to the bedrock surface. The succession shows similar properties to the basal sediments encountered by Dehnert et al. (2012), Buechi

et al. (2017), and Schwenk et al. (2022). These deposits were also interpreted by them as ice-contact sediments at the transition to glaciolacustrine deposition. This transition is represented in the recovered sediment succession by a massive clay bed (Fig. 5j).

– *Subunit A2 (249.7–0128.7 mtd)*. This section is interpreted to have been deposited in a glaciolacustrine setting and consists of the following: (i) thick to medium bedded sand-dominated hyperconcentrated to concentrated density-flow deposits (Table 1; *Sm* and *Sh*; Mulder and Alexander, 2001); (ii) massive gravel-dominated beds, likely high-concentration channelized density-flow deposits (*Gms*), originating from a subaqueous glacial fan system (Eyles et al., 1983); and (iii) a succession of rather thin-bedded to laminated sands of likely turbiditic origin (*Sl* and *Sc*; Mulder and Alexander, 2001; Bouma, 1962). This turbiditic succession separates the partially interbedded sand-dominated and gravel-dominated density-flow deposits into a lower and upper succession, and the latter is terminated by a massive gravel bed. Since these sharp changes in grain size and bedding, frequently observed in this unit, are likely directly related to the flow energy, they may also indicate a lateral variation of the glacier outlet or local subaquatic channel-levee patterns along the submerged proglacial front. Thus, the long-term grain-size evolution controlled by glacier proximity is superimposed by higher-frequency changes caused by local variations in this highly dynamic setting of the glacier front. Therefore, it is unclear if the laminated to partially cross-bedded succession represents a rather lacustrine environment with a more distal-located glacier or a low-energy endmember of the lateral changing depositional system.

– *Subunit A3 (128.7–103.2 mtd)*. The succession of tightly interbedded sand (Table 1; *Sh*) and gravel (*Gms*) beds shows a partially diamictic character (*Dms, Mcc,* and *Sil*). These gravel-rich beds possibly represent slumps and subaquatic mass movements originating on unstable slopes of the rapidly infilling basin (e.g., deltas). The collapse of these unstable slop deposits could be linked to increased sediment flux caused by increased fluvial activity (e.g., glacial outburst floods), an advancing glacial front, or even earthquake shaking. The section shows traces of likely glaciotectonic overprinting (*Sd*, ductile and brittle deformation structures). Further, the top contact of this succession is built by a strongly ductile deformed and/or folded sand bed (*Sd*).

– *Subunit A4 (103.2–91.0 mtd)*. This upper diamictic succession (Table 1; *Dcm*) is similar to the basal one of Subunit A1 but lacks a massive clay bed on top (Fig. 5e and 5j). The upper diamict is also interpreted as subglacial deposits, possibly representing another period of ice contact or at least ice proximity. The sharp and high-frequency changes in grain size of the diamict's top (*Sil, Dcm,* and *Fm*) indicate a partially high-energy but unstable environment. This transition is possibly related to pulsing channelized glacial meltwater outbursts that prevented the deposition of a massive clay bed here.

– *Subunit A5 (91.0–47.7 mtd)*. Subunit A5 is similar to the lower glaciolacustrine section of Subunit A2. However, the overall absence of the massive gravel beds indicates a shift to a more glaciolacustrine-to-lacustrine environment where the depositional energy was lower. Moreover, the succession shows some sections enriched in dropstones (Fig. 5c), pointing to a distal ice-contact lake environment. The whole sediment succession of Unit A is sharply cut off by the sediments of Unit B.

5.1.2 Unit B (47.75–11.00 mtd): fluvial gravel

The sediments of Unit B are interpreted as fluvial-to-glaciofluvial gravels (Table 1; *Gms* and *Gmf*). On the basis of the geographical and stratigraphic position, they are correlated with the local gravel formation "Buechberg Gravel Complex", which also covers the surrounding areas and is interpreted as a Middle Pleistocene advance gravel (Graf, 2009b; Müller, 2013). Further, the relief of the contact surface between Unit A and Unit B indicates a strong fluvial erosion of the former top sediments of Unit A during the deposition of the gravels of Unit B (see Sect. 2 "Study area"; Graf, 2009b; Müller, 2013).

5.1.3 Unit C (11.00–0.00 mtd): glaciogenic diamicts

The sediments of Unit C are interpreted as a subglacial till and associated glaciogenic diamicts (Table 1; *Dmm* and *Dcm*). This interpretation is supported by the following: (i) the high density and consolidation; (ii) the diamictic texture (e.g., Evans et al., 2006; Evans, 2018); (iii) the abundance of fresh traces of direct ice-contact transportation (e.g., striated and/or bullet-shaped clasts, e.g., Evans et al., 2006; Evans, 2018); and (iv) the stratigraphic position. As the drill site is located within the LGM extent of the former Rhine Glacier (Fig. 1a), at least the upper part, if not all of Unit C, was emplaced during the LGM glaciation (Birrfeld glaciation). Alternatively, the lower parts of Unit C may have been emplaced during earlier glaciations that reached the area, e.g., during MIS6 (Beringen glaciation, e.g., Müller, 2013; where MIS represents marine isotope stage). However, a clear unconformity was not observed in the recovered diamicts.

5.2 Implications for glacial history

Assuming that each glacial cycle may have left glacial deposits behind, the two diamictic deposits (Subunits A1

and A4) encountered in an overdeepened position may indicate the presence of at least two glacial sedimentary sequences within Unit A with a sequence boundary between ∼ 103 and 91 mtd (Subunit A4). This interpretation is supported by the presence of glaciotectonic deformations and pressure-related dewatering structures between 128.7–103.2 mtd (Subunit A3), which may have been caused by an overriding glacier during a next glacial cycle. The postulated glacial sequence boundary potentially coincides with the depth of a prominent erosive discontinuity observed in the seismic data (solid dark blue line in Fig. 1c; Brandt, 2020). This coincidence supports the interpretation that a second glacier advance is documented in the upper part of the Basadingen Through, which apparently eroded more into the width while not removing the deeper basin fill. Future age constraints will place these successions in the context of the marine isotope stages.

Since the whole succession of Unit A was deposited mostly under glacial to glaciolacustrine conditions, the lack of a significant amount of clay- and silt-rich glaciolacustrine background sediments (*Fm*) has been rather surprising. This disparity may be explained by either of the following: (i) no considerable amount of such sediments were deposited since the accommodation space was quickly filled by the sandy and gravelly sediments or (ii) they were eroded after deposition as a former presence is at least indicated by the occurrence of mud–clast conglomerates (*Mcc*, rich in clay and silt rip-up clasts). Likely, both processes may have acted together in the assumed high-energy and clastic-dominated glaciolacustrine environment.

In addition to the lack of fine-grained glaciolacustrine deposits, the absence of the fine-grained interstadial/interglacial lacustrine deposits is likely explained by the following: (i) the possibility that the lake never developed such a state as it became rapidly filled in late glacial periods, (ii) by cold and/or short interstadials, or (iii) if deposited initially they were eroded during the next glacial advance. In the case of the proposed lower glacial cycle below 103.2 mtd, the first or second case may apply since the observed increased appearance of diamictic slumps and subaquatic mass-movement deposits between 128.7–103.2 mtd may indicate a rapid glacial readvance after a short interstadial. However, in the case of the proposed upper cycle, the third explanation might act since at least its top was eroded to a certain degree by the overlying gravels of Unit B. Based on these observations, the proposed lower cycle may be, even if not completely preserved, at least more complete than the proposed upper cycle.

However, the existence of such significant "cold" or "warm" lacustrine deposits can not be ruled out for the whole Basadingen Trough since (i) this observation is only based on information from one drill hole; (ii) the assumed highly variable depositional environment; and (iii) due to possible spatial effects, which may impact the probability of local accumulation of such deposits (e.g., subaquatic channels or subaquatic deltas).

The overlying gravels and tills of Units B and C are documenting the glaciation history after the filling of the trough. The gravels of Unit B document the presence of a glacier upstream of the drill site on at least one occasion before it was covered at least once again during the LGM advance of the Rhine Glacier. Whether more than one glacial cycle is preserved in Units B and C, as suggested by Graf (2009b) and Müller (2013), will be addressed with the planned geochronological analysis.

6 Summary and outlook

The proposed complex based on seismic data, possibly multiphase sedimentary fill of the Basadingen Trough (Fig. 1c; Anselmetti et al., 2022; Brandt, 2020), is fully supported by the drilled and recovered succession, even though the bedrock, predicted at ∼ 240 m, was not reached with the final depth of 252 m. It is currently unclear if this is due to an inaccurate identification of the bedrock reflection or to an inaccurate velocity model. Analyzing the vertical seismic profile (VSP) will reveal more details on the bedrock's location. However, the appearance of cobble-sized freshwater molasse fragments indicates the nearby occurrence of the bedrock contact. A first correlation of the drilled succession with the seismic interpretation indicates the coincidence of the glacial depositional sequence at ∼ 103 mtd or ∼ 340 m a.s.l. with the seismic sequence boundary (Figs. 1c and 4; Brandt, 2020), indicating that the Rhine Glacier advanced over the upper part of the Basadingen Trough at that time. This pattern further supports the sedimentary succession's proposed multiphase origin in at least two glacial cycles (Anselmetti et al., 2022). Furthermore, the lacustrine (overdeepened) character of the sediments of Subunit A5 indicates a higher fluvial base level at that time, as was proposed by Graf (2009b) and Müller (2013).

Upcoming correlations of seismic, wireline, and core data will help to establish a robust model of the evolution of the Basadingen Trough. The systematical correlation and characterization of the sedimentological core properties with the extended geophysical and geochemical dataset will refine the definition of glacial sequence stratigraphy that can eventually be dated by the planned geochronological data. This will contribute to the understanding of the local and regional glaciation history, the formation of overdeepenings in the Alpine foreland, and (within the context of DOVE) glaciation and landscape evolution of the Alps.

Data availability. The DOVE operational dataset is published under https://doi.org/10.5880/ICDP.5068.001 (DOVE-Phase 1 Scientific Team et al., 2023b) together with the operational report (DOVE-Phase 1 Scientific Team et al., 2023a) and the explanatory remarks (DOVE-Phase 1 Scientific Team et al., 2023c).

Information on the project and the data is also available on the ICDP DOVE project website: https://www.icdp-online.org/projects/by-continent/europe/dove-switzerland.

Sample availability. IGSNs are assigned to the hole and sample material; samples are available upon request; for further information, see the operational dataset (Dove-Phase 1 Scientific Team et al., 2023b) and the operational report (DOVE-Phase 1 Scientific Team et al., 2023a).

Author contributions. SS served as the leading drill site geologist during the drilling operation, had the lead in the ICD, analyzed the data, and was the main author of the paper with the support of FSA and MWB. BS helped as a substitute drill site geologist and contributed substantially to the ICD. MWB and FSA organized the drilling campaign, operated as substitute drill site geologists, provided support and advice for SS during the drilling operation and the ICD, and provided significant scientific input to the paper as part of their role as PhD supervisors of SS. All authors approved the text and the figures.

Competing interests. The contact author has declared that none of the authors has any competing interests.

Disclaimer. Publisher's note: Copernicus Publications remains neutral with regard to jurisdictional claims in published maps and institutional affiliations.

Acknowledgements. We are grateful for continuing support of the International Scientific Continental Drilling Program (ICDP), including the ICDP Operational Support Group for providing the on-site MSCL scanner and the database management tool "mDis". We acknowledge the tremendous effort of the drilling company, Fretus AG, in particular the drilling crew (Juan Gonzalez, Marek Bajcura, Joaquim Teixeira) for providing us with high-quality drill cores, as well as the technical staff of LIAG, who assisted with the seismic pre-site surveys and the downhole logging. Further, we acknowledge the strong support by the members of the Bürgergemeinde Basadingen-Schlattingen, the members of the Jagdgesellschaft Hegi Belzhalden, the local inhabitants, the involved services of the political community Basadingen-Schlattingen, and the Canton of Thurgau. A special thanks goes to Luka Seslak (our technical drilling consultant), Julijana Gajic, Patrizia Ruffiner (for processing and analyzing the TIC and TOC samples), Kim Lemke (for core transport and support on the drill site), and to the whole DOVE science team for their effort to make this project happen and for keeping it running.

Financial support. This research has been supported by the ICDP, the Deutsche Forschungsgemeinschaft (DFG, grant nos. KR2073/3-1, BU 2467/1-2, GA749/5-1, BU 2467/3-1, BU 3894/2-1, BU 3894/3-1, and PR 957/6-1), Nagra, ENSI, LGRB, LFU, LIAG, BOKU Vienna, and University of Bern.

Review statement. This paper was edited by Nadine Hallmann and reviewed by Bernd Wagner and Pierre Dietrich.

References

Alley, R. B., Cuffey, K. M., and Zoet, L. K.: Glacial erosion: status and outlook, Ann. Glaciol., 60, 1–13, https://doi.org/10.1017/aog.2019.38, 2019.

Anselmetti, F. S., Bavec, M., Crouzet, C., Fiebig, M., Gabriel, G., Preusser, F., Ravazzi, C., and DOVE scientific team: Drilling Overdeepened Alpine Valleys (ICDP-DOVE): quantifying the age, extent, and environmental impact of Alpine glaciations, Sci. Dril., 31, 51–70, https://doi.org/10.5194/sd-31-51-2022, 2022.

Bouma, A. H.: Sedimentology of some Flysch deposits: a graphic approach to facies interpretation, Elsevier, Amsterdam, the Netherlands, https://lib.ugent.be/catalog/rug01:000978747 (last access: 21 September 2023), 1962.

Brandt, A. C.: Erkundung des alpinen, glazial-übertieften Basadingen-Beckens mithilfe von P-Wellen-Seismik, BSc thesis, Leibniz Universität Hannover, unpublished, 2020.

Buechi, M. W., Frank, S. M., Graf, H. R., Menzies, J., and Anselmetti, F. S.: Subglacial emplacement of tills and meltwater deposits at the base of overdeepened bedrock troughs, Sedimentology, 64, 658–685, https://doi.org/10.1111/sed.12319, 2017.

Buechi, M. W., Graf, H. R., Haldimann, P., Lowick, S. E., and Anselmetti, F. S.: Multiple Quaternary erosion and infill cycles in overdeepened basins of the northern Alpine foreland, Swiss J. Geosci., 111, 133–167, https://doi.org/10.1007/s00015-017-0289-9, 2018.

Clark, P. U., Archer, D., Pollard, D., Blum, J. D., Rial, J. A., Brovkin, V., Mix, A. C., Pisias, N. G., and Roy, M.: The middle Pleistocene transition: characteristics, mechanisms, and implications for long-term changes in atmospheric pCO_2, Quaternary Sci. Rev., 25, 3150–3184, https://doi.org/10.1016/j.quascirev.2006.07.008, 2006.

Cohen, D., Gillet-Chaulet, F., Haeberli, W., Machguth, H., and Fischer, U. H.: Numerical reconstructions of the flow and basal conditions of the Rhine glacier, European Central Alps, at the Last Glacial Maximum, The Cryosphere, 12, 2515–2544, https://doi.org/10.5194/tc-12-2515-2018, 2018.

Cook, S. J. and Swift, D. A.: Subglacial basins: Their origin and importance in glacial systems and landscapes, Earth-Sci. Rev., 115, 332–372, https://doi.org/10.1016/j.earscirev.2012.09.009, 2012.

Dehnert, A., Lowick, S. E., Preusser, F., Anselmetti, F. S., Drescher-Schneider, R., Graf, H. R., Heller, F., Horstmeyer, H., Kemna, H. A., Nowaczyk, N. R., Züger, A., and Furrer, H.: Evolution of an overdeepened trough in the northern Alpine Foreland at Niederweningen, Switzerland, Quaternary Sci. Rev., 34, 127–145, https://doi.org/10.1016/j.quascirev.2011.12.015, 2012.

DOVE-Phase 1 Scientific Team, Anselmetti, F. S., Beraus, S., Buechi, M. W., Buness, H., Burschil, T., Fiebig, M., Firla, G., Gabriel, G., Gegg, L., Grelle, T., Heeschen, K., Kroemer, E., Lehne, C., Lu¨thgens, C., Neuhuber, S., Preusser, F., Schaller, S., Schmalfuss, C., Schuster, B., Tanner, D. C.,

Thomas, C., Tomonaga, Y., Wieland-Schuster, U., and Wonik, T.: Drilling Overdeepened Alpine Valleys (DOVE) – Operational Report of Phase 1, (ICDP Operational Report), GFZ German Research Centre for Geosciences, Potsdam, 70 pp., https://doi.org/10.48440/ICDP.5068.001, 2023a.

DOVE-Phase 1 Scientific Team, Anselmetti, F. S., Beraus, S., Buechi, M. W., Buness, H., Burschil, T., Fiebig, M., Firla, G., Gabriel, G., Gegg, L., Grelle, T., Heeschen, K., Kroemer, E., Lehne, C., Lüthgens, C., Neuhuber, S., Preusser, F., Schaller, S., Schmalfuss, C., Schuster, B., Tanner, D. C., Thomas, C., Tomonaga, Y., Wieland-Schuster, U., and Wonik, T.: Drilling Overdeepened Alpine Valleys (DOVE) – Operational Dataset of DOVE Phase 1, GFZ Data Services [data set], https://doi.org/10.5880/ICDP.5068.001, 2023b.

DOVE-Phase 1 Scientific Team, Anselmetti, F. S., Beraus, S., Buechi, M. W., Buness, H., Burschil, T., Fiebig, M., Firla, G., Gabriel, G., Gegg, L., Grelle, T., Heeschen, K., Kroemer, E., Lehne, C., Lu¨thgens, C., Neuhuber, S., Preusser, F., Schaller, S., Schmalfuss, C., Schuster, B., Tanner, D. C., Thomas, C., Tomonaga, Y., Wieland-Schuster, U., and Wonik, T.: Drilling Overdeepened Alpine Valleys (DOVE) – Explanatory remarks on the operational dataset, ICDP Operational Dataset – Explanatory Remarks, GFZ German Research Centre for Geosciences, Potsdam, 34 pp., https://doi.org/10.48440/ICDP.5068.002, 2023c.

Ellwanger, D., Wielandt-Schuster, U., Franz, M., and Simon, T.: The Quaternary of the southwest German Alpine Foreland (Bodensee-Oberschwaben, Baden-Württemberg, Southwest Germany), E&G Quaternary Sci. J., 60, 22, https://doi.org/10.3285/eg.60.2-3.07, 2011.

Evans, D.: Till: A Glacial Process Sedimentology, John Wiley & Sons, Chichester, 383 pp., https://doi.org/10.1002/9781118652541, 2018.

Evans, D. J. A., Phillips, E. R., Hiemstra, J. F., and Auton, C. A.: Subglacial till: Formation, sedimentary characteristics and classification, Earth-Sci. Rev., 78, 115–176, https://doi.org/10.1016/j.earscirev.2006.04.001, 2006.

Eyles, N., Eyles, C. H., and Miall, A. D.: Lithofacies types and vertical profile models; an alternative approach to the description and environmental interpretation of glacial diamict and diamictite sequences, Sedimentology, 30, 393–410, https://doi.org/10.1111/j.1365-3091.1983.tb00679.x, 1983.

Fabbri, S. C., Affentranger, C., Krastel, S., Lindhorst, K., Wessels, M., Madritsch, H., Allenbach, R., Herwegh, M., Heuberger, S., Wielandt-Schuster, U., Pomella, H., Schwestermann, T., and Anselmetti, F. S.: Active Faulting in Lake Constance (Austria, Germany, Switzerland) Unraveled by Multi-Vintage Reflection Seismic Data, Front. Earth Sci., 9, 670532, https://doi.org/10.3389/feart.2021.670532, 2021.

Fiebig, M., Herbst, P., Drescher-Schneider, R., Lüthgens, C., Lomax, J., and Doppler, G.: Some remarks about a new Last Glacial record from the western Salzach foreland glacier basin (Southern Germany), Quatern. Int., 328–329, 107–119, https://doi.org/10.1016/j.quaint.2013.12.048, 2014.

Fitzsimons, S. and Howarth, J.: Chapter 9 – Glaciolacustrine Processes, in: Past Glacial Environments (Second Edition), edited by: Menzies, J. and van der Meer, J. J. M., Elsevier, 309–334, https://doi.org/10.1016/B978-0-08-100524-8.00009-9, 2018.

Graf, H. R.: Stratigraphie und Morphogenese von frühpleistozänen Ablagerungen zwischen Bodensee und Klettgau, E&G Quaternary Sci. J., 58, 12–54, https://doi.org/10.3285/eg.58.1.02, 2009a.

Graf, H. R.: Stratigraphie von Mittel- und Spätpleistozän in der Nordschweiz. Beiträge zur Geologischen Karte der Schweiz (N.F.), 168, Landesgeologie, Swisstopo, 2009b.

Gribenski, N., Valla, P. G., Preusser, F., Roattino, T., Crouzet, C., and Buoncristiani, J.-F.: Out-of-phase Late Pleistocene glacial maxima in the Western Alps reflect past changes in North Atlantic atmospheric circulation, Geology, 49, 1096–1101, https://doi.org/10.1130/G48688.1, 2021.

Haeuselmann, P., Granger, D. E., Jeannin, P.-Y., and Lauritzen, S.-E.: Abrupt glacial valley incision at 0.8 Ma dated from cave deposits in Switzerland, Geology, 35, 143–146, https://doi.org/10.1130/G23094A, 2007.

Hofmann, F.: Erläuterungen zu: Geologischer Atlas der Schweiz – 1052 Andelfingen (Atlasblatt 52), Schweiz. Geol. Komm., 1967.

Hofmann, F. and Hantke, R.: Erläuterungen zu Blatt 1032 Diessenhofen des geologischen Atlas der Schweiz, Schweiz. Geol. Komm., 1964.

Ivy-Ochs, S., Kerschner, H., Reuther, A., Preusser, F., Heine, K., Maisch, M., Kubik, P. W., and Schlüchter, C.: Chronology of the last glacial cycle in the European Alps, J. Quaternary Sci., 23, 559–573, https://doi.org/10.1002/jqs.1202, 2008.

Keller, O. and Krayss, E.: The rhine-linth glacier in the upper wurm: A model of the last alpine glaciation, Quatern. Int., 18, 15–27, https://doi.org/10.1016/1040-6182(93)90049-L, 1993.

Leemann, A. and Niessen, F.: Holocene glacial activity and climatic variations in the Swiss Alps: reconstructing a continuous record from proglacial lake sediments, Holocene, 4, 259–268, https://doi.org/10.1177/095968369400400305, 1994.

Li, S., Li, S., Shan, X., Gong, C., and Yu, X.: Classification, formation, and transport mechanisms of mud clasts, Int. Geol. Rev., 59, 1609–1620, https://doi.org/10.1080/00206814.2017.1287014, 2017.

Lisiecki, L. E. and Raymo, M. E.: Pliocene-Pleistocene stack of globally distributed benthic stable oxygen isotope records, PANGAEA [data set], https://doi.org/10.1594/PANGAEA.704257, 2005.

Lønne, I.: Sedimentary facies and depositional architecture of ice-contact glaciomarine systems, Sediment. Geol., 98, 13–43, https://doi.org/10.1016/0037-0738(95)00025-4, 1995.

Meyers, P. A. and Teranes, J. L.: Sediment Organic Matter, in: Tracking Environmental Change Using Lake Sediments: Physical and Geochemical Methods, edited by: Last, W. M. and Smol, J. P., Springer Netherlands, Dordrecht, 239–269, https://doi.org/10.1007/0-306-47670-3_9, 2001.

Mulder, T. and Alexander, J.: The physical character of subaqueous sedimentary density flows and their deposits, Sedimentology, 48, 269–299, https://doi.org/10.1046/j.1365-3091.2001.00360.x, 2001.

Müller, E. R.: Mittelpleistozäne Schottervorkommen zwischen dem Thurtal und Schaffhausen, Swiss Bulletin für angewante Geologie, 18/1, 3–27, ETH Zürich, https://doi.org/10.5169/SEALS-391135, 2013.

Penck, A. and Brückner, E.: Die Alpen im Eiszeitalter, Tauchnitz, Leibzig, 1909.

Pietsch, J. and Jordan, P.: Digitales Höhenmodell Basis Quartär der Nordschweiz – Version 2014 und ausgewählte Auswertungen, Nagra Arbeitsber. NAB 14-02, 2014.

Pomper, J., Salcher, B. C., Eichkitz, C., Prasicek, G., Lang, A., Lindner, M., and Götz, J.: The glacially overdeepened trough of the Salzach Valley, Austria: Bedrock geometry and sedimentary fill of a major Alpine subglacial basin, Geomorphology, 295, 147–158, https://doi.org/10.1016/j.geomorph.2017.07.009, 2017.

Preusser, F., Reitner, J. M., and Schlüchter, C.: Distribution, geometry, age and origin of overdeepened valleys and basins in the Alps and their foreland, Swiss J. Geosci., 103, 407–426, https://doi.org/10.1007/s00015-010-0044-y, 2010.

Preusser, F., Graf, H. R., Keller, O., Krayss, E., and Schlüchter, C.: Quaternary glaciation history of northern Switzerland, E&G Quaternary Sci. J., 60, 21, https://doi.org/10.3285/eg.60.2-3.06, 2011.

Reber, R. and Schlunegger, F.: Unravelling the moisture sources of the Alpine glaciers using tunnel valleys as constraints, Terra Nova, 28, 202–211, https://doi.org/10.1111/ter.12211, 2016.

Ruddiman, W. F., Raymo, M., and McIntyre, A.: Matuyama 41 000-year cycles: North Atlantic Ocean and northern hemisphere ice sheets, Earth Planet. Sci. Lett., 80, 117–129, https://doi.org/10.1016/0012-821X(86)90024-5, 1986.

Schaller, S., Böttcher, M. E., Buechi, M. W., Epp, L. S., Fabbri, S. C., Gribenski, N., Harms, U., Krastel, S., Liebezeit, A., Lindhorst, K., Marxen, H., Raschke, U., Schleheck, D., Schmiedinger, I., Schwalb, A., Vogel, H., Wessels, M., and Anselmetti, F. S.: Postglacial evolution of Lake Constance: sedimentological and geochemical evidence from a deep-basin sediment core, Swiss J. Geosci., 115, 7, https://doi.org/10.1186/s00015-022-00412-1, 2022.

Schlüchter, C.: The Swiss glacial record – a schematic summary, in: Developments in Quaternary Sciences, Elsevier, vol. 2, 413–418, https://doi.org/10.1016/S1571-0866(04)80092-7, 2004.

Schwenk, M. A., Schläfli, P., Bandou, D., Gribenski, N., Douillet, G. A., and Schlunegger, F.: From glacial erosion to basin overfill: a 240 m-thick overdeepening–fill sequence in Bern, Switzerland, Sci. Dril., 30, 17–42, https://doi.org/10.5194/sd-30-17-2022, 2022.

Spötl, C., Koltai, G., Jarosch, A. H., and Cheng, H.: Increased autumn and winter precipitation during the Last Glacial Maximum in the European Alps, Nat. Commun., 12, 1839, https://doi.org/10.1038/s41467-021-22090-7, 2021.

Valla, P. G., Shuster, D. L., and van der Beek, P. A.: Significant increase in relief of the European Alps during mid-Pleistocene glaciations, Nat. Geosci., 4, 688–692, https://doi.org/10.1038/ngeo1242, 2011.